Chapter 3

Characterization of DNA-bound Dps

3.1 Introduction

Dps proteins are dodecameric (12-mer) bacterial ferritins that protect DNA from oxidative stress, and have been implicated in bacterial survival and virulence (*1*). This protection is thought to derive from ferroxidase activity, wherein Dps proteins simultaneously deplete ferrous iron and hydrogen peroxide, reactive species that can otherwise form damaging hydroxyl radicals via Fenton chemistry (*2*). Like other ferritins, Dps proteins are spherical, with a hollow core where oxidized iron is reversibly stored. Some Dps proteins also nonspecifically bind DNA, such as that from *E. coli* which utilizes N-terminal lysine residues for DNA binding (*3*). Within cells, Dps is upregulated by the transcriptional regulator OxyR in response to oxidative stress (*1*), and is also upregulated in stationary phase, when an additional physical component of Dps protection is biocrystallization with DNA (*4*).

DNA charge transport (CT), wherein both electrons and electron holes are efficiently transported through the base-pair π-stack, can be used biologically by proteins, both as a first step for 4Fe4S cluster-containing DNA repair proteins to localize to the vicinity of a lesion within the vast milieu of the genome, and for the selective activation of redox-active transcription factors from a distance (*5*). In addition to direct interaction with diffusing oxidants, could Dps proteins utilize DNA CT to protect DNA from a distance? Guanine is the most easily oxidized base within the DNA, and the presence of adjacent guanines further lowers the guanine oxidation potential (*6*); thus, radicals are characteristically formed at guanine multiplets upon DNA photooxidation (*7*,*8*). A long distance protection mechanism

via DNA CT would involve electron transfer from Dps through the DNA π-stack to fill the hole on guanine radicals, restoring the integrity of the DNA. In this way, Dps could respond to an oxidative affront to the DNA, even if the protein is bound, at the minimum, a hundred base-pairs away (*9*).

Indeed, we have previously shown that *E. coli* Dps loaded with ferrous iron can protect DNA from oxidative damage created through the flash-quench technique (*10*). The intercalating photooxidant $[Ru(phen)(dppz)(bpy')]^{2+}$, where phen is 1,10-phenanthroline and bpy′ is 4-butyric acid-4′-methyl-2,2′-bipyridine, was covalently tethered the 5′ end of mixed-sequence 70-mer DNA. Upon excitation with visible light ("flash"), the ruthenium(II) excited state can be oxidatively quenched ("quench") by a diffusing quencher, such as $[Co(NH_3)_5Cl]^{2+}$, to form a highly oxidizing intercalated Ru(III) complex (1.6 V versus NHE) (*11*). In the absence of protein, oxidative damage is observed preferentially at a guanine triplet within the 70-mer DNA duplex. Titrating in ferrous iron-loaded Dps significantly attenuates the level of oxidative damage at the guanine triplet, while Apo-Dps and ferric iron-loaded Dps, which lack available reducing equivalents, do not display this protection (*10*). Luminescence experiments rule out direct interaction between the ruthenium photooxidant excited state and Dps, suggesting a DNA-mediated oxidation mechanism. Long-distance, DNA-mediated oxidation of Dps could be an effective mechanism for bacteria to protect their genomes from oxidative insults, perhaps contributing to pathogenic survival and virulence.

The goal of this current work is to spectroscopically characterize the DNA-mediated oxidation of ferrous iron-loaded Dps. Electron paramagnetic resonance (EPR) spectroscopy has previously been used to observe protein oxidation following flash-quench DNA photooxidation. Specifically, EPR studies with MutY, a base excision repair glycosylase with a $[4Fe4S]^{2+}$ cluster as-isolated, compared the homopolymeric DNAs poly(dG-dC) and poly(dA-dT) (*12*). When a sample containing MutY, poly(dG-dC) DNA, $[Ru(phen)_2(dppz)]^{2+}$ and diffusing quencher was irradiated, a mixture of the oxidized $[4Fe4S]^{3+}$ cluster and its decomposition product, $[3Fe4S]^{+}$, was detected with low temperature EPR. When poly(dG-dC) was substituted with poly(dA-dT), a significantly lower intensity EPR signal was observed. Combined with transient absorption experiments, these data directly demonstrated MutY 4Fe4S cluster oxidation by guanine radicals through DNA CT. While MutY can be oxidized to some degree without guanine radical as an intermediate, the thermodynamically favorable oxidation of the MutY $[4Fe4S]^{2+}$ cluster by guanine radical enables more efficient MutY oxidation (*12*).

What type of EPR signal might we expect for Dps? At the inter-subunit ferroxidase sites of Dps, two irons ions are bound by two conserved histidine ligands and two conserved carboxylate ligands, glutamate and aspartate (*1*). This ligand coordination sphere creates two binding sites with very different iron affinities: while one site has a relatively high affinity, the other site binds iron weakly (*13*). After binding, ferrous iron is oxidized and shuttled to the core of the protein for storage. Whereas 24-mer ferritins react rapidly with dioxygen as an oxidant, Dps proteins react slowly with dioxygen and much more quickly with hydrogen

peroxide (*14*). We have previously found that ferricyanide also works well as a chemical oxidant of *E. coli* Dps in solution (*10*). Whereas full occupation of the twelve di-iron centers of the protein would correspond to 24 Fe(II)/Dps, we have found that under the anaerobic conditions used in our experiments (i.e. in the absence of oxidants), *E. coli* Dps binds only 12 Fe(II)/Dps (*10*). This agrees with studies on *Bacillus anthracis* and *Listeria innocua* Dps proteins, where a bridging oxidant seems to be required to tether the lower affinity iron and form the di-iron site (*13*,*15*). Coupled with the specificity of iron binding evidenced by its abrogation in the *E. coli* Dps ferroxidase site double mutant H51G/H63G, the 12 Fe(II)/Dps likely corresponds to binding at the higher affinity iron site of each ferroxidase center in the dodecameric protein. Therefore, in spectroscopic studies with Dps, we would expect to observe the oxidation of mononuclear non-heme iron sites.

Mononuclear high-spin Fe(III) sites of low symmetry (i.e., non-heme) typically display an EPR signal with an apparent *g*-value of 4.3 (*16*,*17*). The ground state of the high-spin d^5 Fe(III) $S = 5/2$ species is split into three Kramer's doublets according to the zero field splitting parameters D and E. In purely rhombic cases, the distortion parameter E/D is equal to 1/3, and the doublets are equally spaced. At low magnetic fields, the spin states mix and the $\Delta M_s = \pm 1$ selection rule no longer holds, allowing for transitions within, rather than between, the Kramer's doublets. The transition within the middle pair of Kramer's doublets ($M_s = \pm 3/2$) produces an isotropic signal at $g = 4.29$. Because of its isotropic nature, this transition produces a strong signal that is easily observed.

This mononuclear high-spin Fe(III) signal at $g = 4.3$ has been frequently reported in the EPR spectra of 24-mer ferritins. For instance, the EPR spectra of horse spleen ferritin oxidized by dioxygen has been described after rapid mixing of aerobic ferritin with an anaerobic solution of ferrous iron (*18*). After varying reaction times, the sample was freeze-quenched and measured at 7.2 K. EPR experiments with iron must typically must be performed at low temperature because of their rapid spin-lattice relaxation. In the early stages of ferrous iron oxidation, mononuclear Fe^{3+}-apoferritin with $g = 4.3$ is formed quantitatively. This signal is followed by the appearance of a mixed-valent Fe^{2+}-Fe^{3+} species with $g = 1.87$, derived from the mononuclear ferric iron sites within the first second of reaction. At later times, as the oxidized iron translocates to the core of the protein, polynuclear EPR-silent Fe^{3+} species are formed (*18*).

Conversely, the EPR spectra of iron-bound Dps proteins have not been previously reported. *Sulfolobus solfataricus* Dps selectively binds two Mn^{2+} as evidenced by EPR titrations (*19*). Spin trapping experiments have been performed with Dps proteins that measure the EPR-active adduct of hydroxyl radical with EMPO (5-ethoxycarbonyl-5-methyl-pyrroline-N-oxide). The presence of both *E. coli* and *Listeria innocua* Dps proteins have been shown to attenuate formation of the EMPO-OH adduct resulting from reaction of ferrous iron and hydrogen peroxide (*13*,*14*).

Here, we use X-band EPR to observe the oxidation of DNA-bound *E. coli* Dps loaded with 12 Fe(II)/Dps. Using the flash-quench technique with non-covalent racemic $[Ru(phen)(dppz)(bpy')]^{2+}$ and the diffusing quencher $[Co(NH_3)_5Cl]^{2+}$, we compare the

alternating copolymers poly(dGdC)$_2$ and poly(dAdT)$_2$ in order to investigate if guanine radical is an important intermediate in Dps oxidation. Thus our goals are to spectroscopically confirm the oxidation of ferrous iron-loaded Dps following DNA photooxidation, and investigate the DNA-mediated characteristics of this oxidation.

We also seek to explore possible electron transfer intermediates in the DNA-mediated oxidation of ferrous iron-loaded Dps. There is a highly conserved tryptophan residue in close proximity (approximately 5 Å) to the ferroxidase site in Dps proteins (Figure 1), W52 in *E. coli*. Because of the location of this aromatic tryptophan residue between the ferroxidase site and the outer protein shell, it is an attractive candidate as a hopping intermediate to facilitate electron transfer between the ferroxidase site of Dps and DNA. While the molecular characteristics of DNA binding are unknown, one proposal suggests that *D. radiodurans* Dps uses its N-terminal extensions to bind to consecutive DNA major grooves along the dimer interface of the dodecamer where the ferroxidase sites are located (*20*). Although *D. radiodurans* Dps has exceptionally long N-terminal extensions that bind Co^{2+}, *E. coli* Dps also has an N-terminal extension that contains three lysine residues as well as an arginine residue. An arginine residue protruding from center helix of *D. radiodurans* Dps (Arg132) is also implicated in DNA binding; in *E. coli*, there is a lysine residue in this position (Lys101). Thus this general DNA-binding mechanism may be conserved from *D. radiodurans* to *E. coli* Dps; if so, W52 would be ideally situated as an electron transfer hopping intermediate. Moreover, this work finds no evidence for DNA wrapping around an individual Dps dodecamer (*20*). As well as the conserved tryptophan residue in Dps

proteins, in 24-mer ferritins there is a conserved tyrosine residue in close proximity to the intrasubunit ferroxidase site.

Previous work has suggested important roles for these conserved aromatic residues in ferritins (*21-24*). Upon oxidation with hydrogen peroxide of Dps loaded with only 6 Fe(II)/Dps, UV-visible stopped flow experiments with *E. coli* Dps were able to observe spectra with maxima at 512 and 536 nm, consistent with a neutral tryptophan radical (*21*). Maximal intensity was reached after 50 ms, and the radical displayed a lifetime of approximately 1700 ms. *L. innocua* Dps proteins additionally contain a tyrosine residue (Y50) approximately 8 Å from the conserved tryptophan residue near the ferroxidase site (W32 in *L. innocua* numbering). Site-directed mutagenesis studies with *L. innocua* Dps were able to confirm the identity of the radicals: Y50R Dps exhibited only tryptophan radical spectra, W32L Dps exhibited only tyrosine radical spectra, and the Y50R/W32L double mutant displayed neither spectra. By comparison with these *L. innocua* Dps results, Bellapadrona *et al.* were able to ascribe the tryptophan radical in *E. coli* to W52 (*21*). Interestingly, the ability of the WT and mutant *L. innocua* Dps to protect plasmid DNA from degradation by ferrous iron and hydrogen peroxide was investigated. Whereas the single W32L mutation did not inhibit the protection capacity of *L. innocua* Dps and the Y50R mutation inhibited this protection only slightly, in the double mutant, Y50R/W32L, the protective capacity of *L. innocua* Dps was significantly attenuated. Bellapadrona *et al.* concluded that these conserved aromatic residues act as a trap for electron holes generated by the oxidation of insufficient ferrous iron by hydrogen peroxide (*21*). That is, the reduction

of hydrogen peroxide to water is a two electron process, but this study was conducted under iron loading conditions where the high affinity iron site is only partially occupied, precluding formation of the di-iron site that would provide two electrons. Thus these aromatic residues seem to provide the extra electron that may otherwise be abstracted from DNA, resulting in oxidative damage (*21*).

In 24-mer ferritins, a tyrosine radical has been observed with EPR upon aerobic incubation of the Apo-protein with ferrous iron in human H-chain ferritin (*22*,*23*), horse spleen ferritin (*18*), *E. coli* bacterial ferritin (24-mer) (*24*), and archaeal *Pyrococcus furiosus* ferritin (*23*). This radical has been ascribed to the conserved tyrosine residue near the ferroxidase site by site-directed mutagenesis studies (*22*,*24*). A study on human H-chain ferritin and *P. furiosus* ferritin proposed a universal mechanism for 24-mer ferritins, wherein the conserved tyrosine residue acts as a molecular capacitor, facilitating oxidation of ferrous iron at the ferroxidase sites by providing an extra electron for the reduction of dioxygen to water (*23*). When this tyrosine residue was mutated to phenylalanine in both proteins, key intermediates in iron oxidation (μ-peroxo-diferric intermediate) were absent and the rate of ferrous iron oxidation at the ferroxidase sites was significantly decreased (*23*). This proposal for tyrosine as a molecular capacitor in 24-mer ferritins is similar to the role proposed for W52 in *E. coli* Dps (*21*). However, other studies with 24-mer ferritins contend with a universal mechanism (*24*). Experiments with *E. coli* bacterial ferritin find that a tyrosine to phenylalanine mutant is able to form the μ-peroxo-diferric intermediate similarly to the WT protein, but that oxidation is slowed upon further addition of ferrous iron to the protein

(*24*). These researchers therefore suggest a possible redox or structural role for the conserved tyrosine residue in the assembly of the oxidized iron core. Overall, it is clear that the conserved aromatic residue in close proximity to the ferroxidase site may play an important role in ferritins.

Here, we investigate two *E. coli* Dps W52 mutants: W52Y, where an aromatic residue is maintained at this position, and W52A, which abolishes the aromatic residue adjacent to the ferroxidase site. We compare these mutants with the WT protein in EPR studies of the oxidation of ferrous iron-loaded Dps following DNA photooxidation. Because the intercalating ruthenium photooxidant is a one-electron oxidant, sending one electron hole at a time into the DNA π-stack, we will be examining the role of *E. coli* Dps W52 as an electron transfer hopping intermediate rather than a molecular capacitor. In addition to EPR, we also probe the role of W52 Dps in cells using a hydrogen peroxide survival assay. Previously, in a *dps* knockout *E. coli* strain (*dps*::*kan* Δ*recA* Δ*ara*), it was demonstrated that induction of WT Dps on a plasmid before exposure to hydrogen peroxide significantly increased bacterial survival compared to un-induced cells (*25*). Additionally, Dps specifically prevents guanine oxidation *in vivo*. Upon treatment with hydrogen peroxide, a CC104 *dps*::*kan* knockout strain displayed a 10-fold increase in GC to TA transversion mutations, caused by 8-oxoG:A mismatches, compared to the strain with WT *dps* (*25*). No increase in mutation frequency was observed for any of the other six possible base substitutions. Furthermore, WT Dps expression from an inducible plasmid was able to partially rescue the number of revertant-causing mutations in CC104 strains with *mutY* and *mutM* knockouts,

which encode DNA glycosylase enzymes (*25*). MutM recognizes 8-oxoG:C pairs and excises the 8-oxoG, while MutY removes adenine from 8-oxoG:A mismatches (*26*). Given these intriguing results, the role of Dps proteins, particularly with regard to a long-distance DNA-mediated protection mechanism, should be further explored *in vivo*.

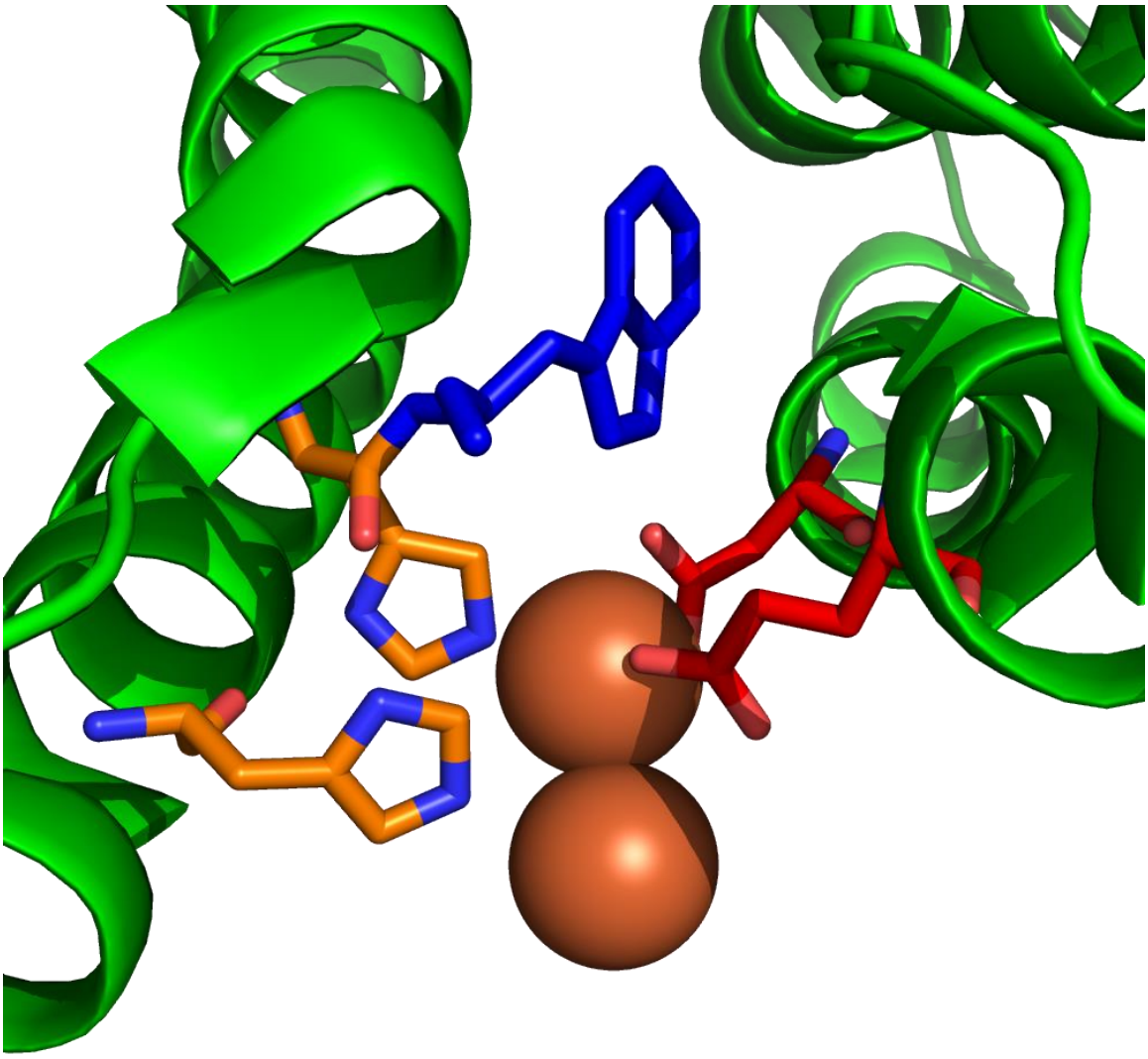

Figure 1. Crystal structure illustrating conserved residues of the ferroxidase site in Dps proteins. The iron ligands are shown in orange (histidines) and red (carboxylates); the conserved tryptophan residue in close proximity to the ferroxidase site is shown in blue. The *E. coli* protein has not been crystallized with bound iron; *Bacillus brevis* Dps shown (PDB: 1N1Q; reference: Ren, B. et al. *J. Mol. Biol.* **2003**, *329*, 467-477).

3.2 Experimental section

3.2.1 W52 mutagenesis

The W52A and W52Y *E. coli* Dps mutants were made with a Quikchange II-E Site-Directed Mutagenesis Kit (Stratagene) using the pBAD18-dps plasmid (containing the WT *E. coli* dps gene and an ampicillin resistance cassette) donated by Dr. Roberto Kolter (*25*) as a template. Primers were purchased from Integrated DNA Technologies. All mutagenized plasmids were sequenced (Laragen) to confirm the desired sequences. After successfully creating the mutant pBAD18-dps plasmids, the *E. coli* cell line ZK2471 (*dps*::*kan* Δ*recA* Δ*ara*) donated by Dr. Roberto Kolter was made electrocompetent and the plasmid was transformed via electroporation into these cells. Primer sequences were as follows, with mutagenized codon underlined:

W52A-forward: 5′-GATCTTTCTTTGATTACCAAACAAGCGCACGCGAACATGC-3′

W52A-reverse: 5′-GCATGTTCGCGTGCGCTTGTTTGGTAATCAAAGAAAGATC-3′

W52Y-forward: 5′-CAGTTTATTGATCTTTCTTTGATTACCAAACAAGCGCACTAC AACATGC-3′

W52Y-reverse: 5′- GCATGTTGTAGTGCGCTTGTTTGGTAATCAAAGAAAGATCAA TAAACTG-3′

3.2.2 CD of WT and mutants

Protein concentrations were determined using ε_{280} values calculated using the ExPASy ProtPram tool (http://web.expasy.org/protparam/). The calculated molar absorptivity values for WT, W52A and W52Y *E. coli* Dps dodecamers were ε_{280} = 185,640

$M^{-1}cm^{-1}$, 119,640 $M^{-1}cm^{-1}$, and 137,520 $M^{-1}cm^{-1}$, respectively. Spectra were recorded at 25°C on a Model 430 circular dichroism spectrometer (AVIV) in a buffer consisting of 50 mM Tris, pH 7.0, 150 mM NaCl. The spectra shown are the average of three individual scans, with a buffer alone spectrum subtracted.

3.2.3 Materials

The alternating co-polymer DNA duplexes poly(dGdC)$_2$ and poly(dAdT)$_2$ were purchased from Sigma. The DNA duplexes were passed through Bio-rad spin columns (6 K MWCO) before use and quantified based on their molar absorptivity values in terms of base-pairs (*27*), (poly(dGdC)$_2$: ε_{254} = 16,800 M^{-1} cm^{-1}, poly(dAdT)$_2$: ε_{262} = 13,200 M^{-1} cm^{-1}). Duplexes were then dried on a speed-vac, brought into an anaerobic chamber (Coy), and re-suspended in deoxygenated buffer.

$[Ru(phen)(dppz)(bpy')]^{2+}$ was synthesized according to published methods (*28*), purified by reversed-phase chromatography, and characterized by NMR and ESI mass spectrometry (expected for the +2 ion: 409.62 m/z, observed: 410.2 m/z). The ruthenium photooxidant was brought into the anaerobic chamber as a solid powder, re-suspended with deoxygenated buffer, and a sample removed for quantification based on UV-Vis absorption (ε_{440} = 21,000 M^{-1} cm^{-1}). $[Co(NH_3)_5Cl]Cl_2$ was purchased from Sigma (99.995% pure) and used as received. The Co quencher was brought into the anaerobic chamber as a solid powder, re-suspended with deoxygenated buffer, and a sample removed for quantification based on UV-Vis (ε_{550} = 47.5 M^{-1} cm^{-1}).

WT and W52 mutant *E. coli* Dps proteins were purified according to previous procedures (*10*). Proteins were deoxygenated in Schlenck tubes according to previous procedures (*10*), and brought into the anaerobic chamber. Proteins were then anaerobically loaded with ferrous iron also according to previous procedures (*10*). Buffers (50 mM Tris or 50 mM MOPS, pH 7.0, 150 mM NaCl, 5% glycerol) were deoxygenated in a Schlenk flask by at least 4 cycles of freeze-pump-thaw.

3.2.4 EPR sample preparation

EPR samples were prepared in an anaerobic chamber (Coy) using the anaerobic materials outlined above. Samples were loaded into EPR tubes within the anaerobic chamber, sealed with septa, and parafilmed around the septa seal. EPR tubes were then brought out of the anaerobic chamber, frozen in liquid nitrogen, and kept in the dark until measurement. Precipitated samples were thoroughly mixed before freezing in liquid nitrogen. For chemically oxidized samples, ferrous iron-loaded protein (approximately 120 μL) was added to the bottom of an EPR tube. Approximately 20 μL of ferricyanide solution was added to the top of the EPR tube, which was then sealed. Upon removal from the anaerobic chamber, the solutions were mixed together and immediately froze in liquid nitrogen within approximately 5-10 seconds of the initiation of mixing.

3.2.5 EPR experiments

EPR spectra were measured on an X-band Bruker EMX spectrometer equipped with an ER4119HS resonator and an Oxford ES9000 cryostat. Instrumental settings are detailed in figure captions, but were generally as follows: modulation amplitude = 10 G at 100 kHz,

frequency = 9.37 GHz, microwave power = 6.4 mW, temperature = 10 K. Samples in Suprasil quartz EPR tubes were irradiated while freezing in liquid nitrogen in an unsilvered Dewar. The excitation source was a xenon lamp equipped with a lens to focus the beam and a 320 nm long-pass filter to remove UV light. Each sample was irradiated for a total of approximately 10 seconds. For each sample, a dark control EPR spectrum was first measured at 10 K. The sample was then thawed, mixed, and irradiated while freezing with liquid nitrogen as described. The EPR spectrum of the irradiated sample was then measured under identical instrumental settings. For data analysis, the dark control spectrum was smoothed and subtracted from the irradiated sample.

3.2.6 Hydrogen peroxide survival experiments

This protocol is adapted from that reported by Martinez and Kolter (*25*). Hydrogen peroxide was purchased from Macron (30% solution) and confirmed to be 10.8 M by $KMnO_4$ titration (*29*). Lyophilized catalase from bovine liver (≥ 20000 units/mg protein) was purchased from Sigma and re-suspended in buffer (50 mM KPO_4, pH 7) to make a stock concentration of 0.4 mg/mL. Overnight cultures of the *E. coli* ZK2471 strain (*dps*::*kan* Δ*recA* Δ*ara*) containing WT, W52A, or W52Y pBAD18-*dps* plasmids were prepared by inoculating single colonies in 5 mL of LB media containing 100 μg/mL ampicillin and 50 μg/mL kanamycin. After overnight shaking at 37°C, the cultures were diluted 1:500 into 50 mL of fresh LB media also containing antibiotics. For each WT, W52A, and W52Y, both induced and un-induced 50 mL cultures were prepared: L-arabinose was added to induce Dps overexpression (0.2% w/v final concentration), and an

equivalent volume of sterile water was added to un-induced cells. Cultures were then incubated at 37°C with shaking (200 rpm) for 3 hours until OD_{600} = 0.3-0.4 (exponential phase). Next, cultures were poured into sterile trays and aliquoted with a multichannel pipette into a sterile 96-well plate (one culture type per row, 200 µL per well, 8 wells in each row). A second 96-well plate was prepared with a row of increasing hydrogen peroxide stock solutions. Hydrogen peroxide solutions were then added with a multichannel pipette (10 µL) and mixed by pipetting. After 15 minutes at RT, catalase solution was added to stop the reaction using a multichannel pipette (5 µL, working concentration: 10 µg/mL culture) and mixed by pipetting. Cultures were incubated for 15 minutes after catalase addition to ensure complete hydrogen peroxide reaction. Cultures were then serially diluted into minimal M63 media for a total of 12,800-fold dilution. Finally, cultures were plated (30 µL) onto LB agar plates containing ampicillin and kanamycin and incubated at 37°C overnight. The number of colonies on each plate were manually counted the subsequent day.

3.3 Results and Discussion

3.3.1 Structure and Fe binding of W52 Dps mutants

The Dps monomer is composed of a four helix bundle with two helix-turn-helix motifs (*30*). The far-UV circular dichroism (CD) spectra of WT Apo-Dps is consistent with this α-helical structure (Figure 2) (*31*). Comparison of the WT with W52A and W52Y Dps CD spectra shows that overall protein folding is relatively unaffected by these mutations. Next, iron binding at the ferroxidase site was investigated for both mutations. As previously described for WT Dps (*10*), the proteins were incubated anaerobically with excess ferrous iron and unbound iron was subsequently removed with size exclusion chromatography. The number of irons bound per Dps dodecamer was then quantified by the formation of $[Fe(bpy)_3]^{2+}$ after protein denaturation and addition of reductant and 2,2′-bipyridine. When Dps concentration is measured via the Bradford reagent or calculated ε_{280} values, the Fe(II)/Dps can be quantified. In one trial, the WT protein bound 14.6 ± 0.5 Fe(II)/Dps, whereas the W52A and W52Y mutants bound only 8.6 ± 0.4 and 10.6 ± 0.4 Fe(II)/Dps, respectively. Similar results were obtained in other trials. Note that small increases from 12 Fe(II)/Dps in the WT protein are likely due to a minor degree of oxidation due to trace oxygen, allowing for some di-iron site formation. Figure 3 shows the $[Fe(bpy)_3]^{2+}$ spectra normalized to protein concentration for WT, W52A, and W52Y Dps. W52A Dps binds iron on the order of 60% of WT, while W52Y is slightly better, binding 70% of the iron of WT Dps. Thus iron binding is somewhat attenuated, but not abrogated, for these mutations.

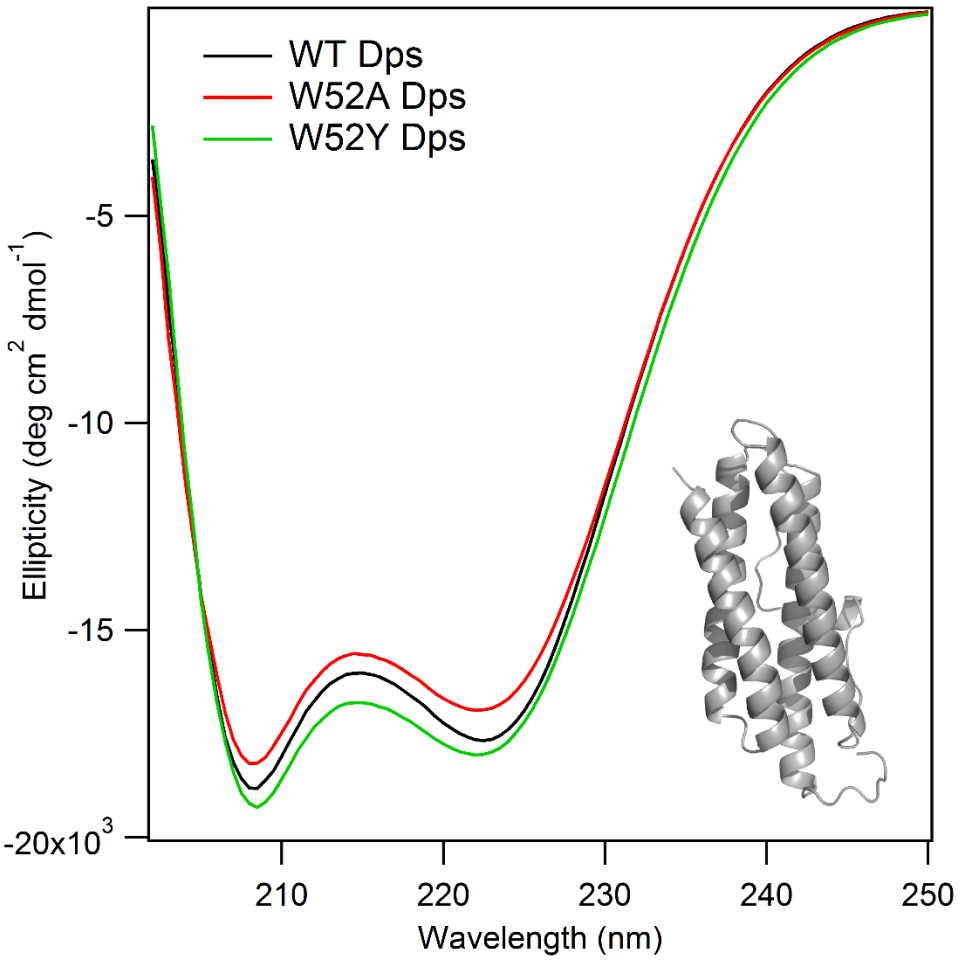

Figure 2. Circular dichroism spectra of wild-type (WT) (black), W52A (red), and W52Y (green) *E. coli* Apo-Dps. Dps monomer depicted in gray, showing α-helical structure. Protein concentration was 5 μM in a buffer of 50 mM Tris, pH 7.0, 150 mM NaCl.

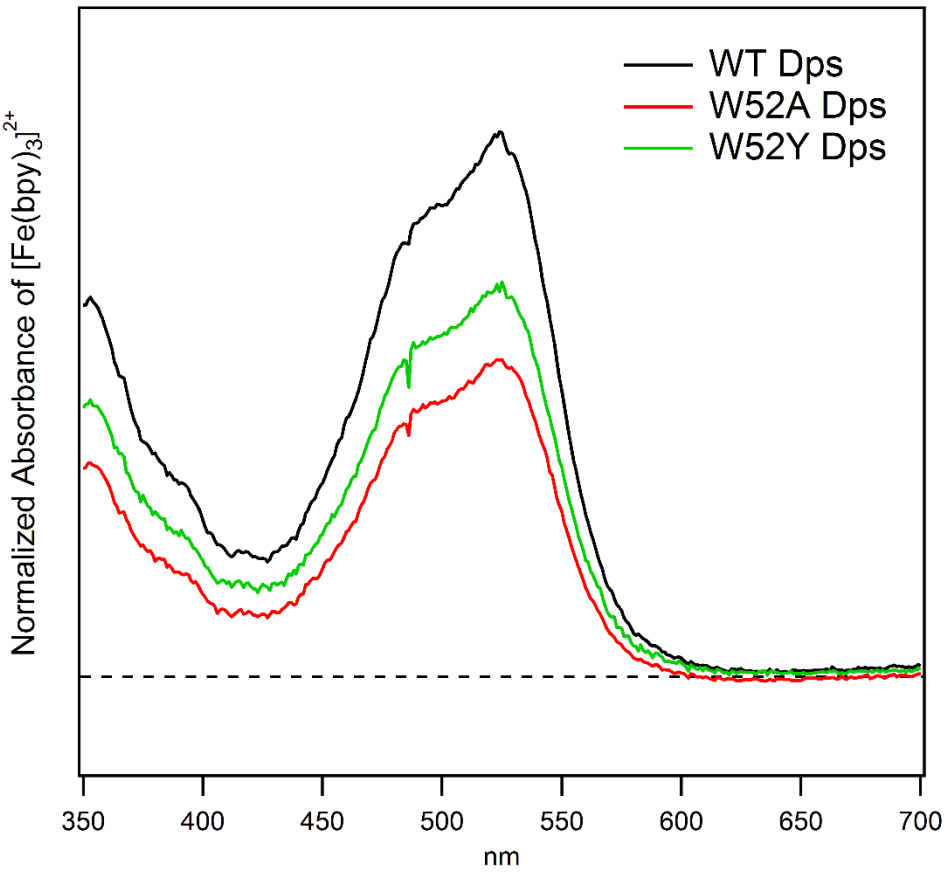

Figure 3. Ferrous iron loading of Dps W52 mutants compared to WT *E. coli* protein. Normalized UV-Visible spectra of $[Fe(bpy)_3]^{2+}$ produced from either WT Dps (black), W52A Dps (red), or W52Y Dps (green). For normalization, the absorbance values were divided by protein concentration. The calculated number of iron atoms per Dps dodecamer is 14.6 ± 0.5 for WT Dps, 8.6 ± 0.4 for W52A, and 10.6 ± 0.4 for W52Y. Protein concentrations were determined by A_{280} using calculated ε_{280} values (185,640 $M^{-1}cm^{-1}$ for WT, 119,640 $M^{-1}cm^{-1}$ for W52A, and 137,520 $M^{-1}cm^{-1}$ for W52Y); the concentration of $[Fe(bpy)_3]^{2+}$ was determined by A_{522} using a derived extinction coefficient of 8,790 $M^{-1}cm^{-1}$.

3.3.2 EPR results with WT *E. coli* Dps

Because the EPR spectrum of iron-bound Dps proteins has not been previously reported, we first used chemical oxidation to confirm the Dps oxidation products to expect in flash-quench studies. All EPR samples described in this study were prepared anaerobically in an anaerobic chamber in order to prevent dioxygen oxidation of ferrous iron loaded Dps. Samples were loaded into EPR tubes and sealed with septa before removal from the anaerobic chamber. As expected, Apo-Dps, which has not been loaded with iron, and Dps loaded with ferrous iron are EPR-silent (Figure 4). However, when WT Dps loaded with 12 Fe(II)/Dps is mixed anaerobically with stoichiometric ferricyanide and frozen in liquid nitrogen within 5-10 seconds, a split signal at $g = 4.3$ is observed at low temperature (10 K) (Figure 4). Given that ferricyanide has a different *g*-value and ferrocyanide is EPR-silent, and that the steady-state UV-Visible spectrum of ferrous iron-loaded Dps incubated with ferricyanide indicates the formation of oxidized iron species (*10*), this signal at $g = 4.3$ can be ascribed to oxidized ferric iron at the mononuclear ferroxidase site in Dps.

As described above, this is the expected EPR signal for mononuclear, non-heme, high-spin Fe(III) sites of low symmetry (*16,17*), and has previously been observed in EPR studies in 24-mer ferritins (*18*). No other EPR-active species are apparent in wide spectra from 500 to 4500 gauss. When instead the ferrous iron-loaded Dps was incubated with ferricyanide for much longer times, no EPR-active species were observed (data not shown), likely because the oxidized iron was translated to the core of the protein, forming EPR-silent polynuclear species.

Next, we investigated the oxidation of DNA-bound WT *E. coli* Dps via the flash-quench technique. Here, the sample is irradiated in an EPR tube while freezing in liquid nitrogen in a clear dewar in order to trap reactive intermediates. Under the conditions used in these experiments, all samples containing both Dps and DNA precipitated, consistent with earlier studies on *E. coli* Dps (*3*). For each sample, an individual dark control (DC) was measured at low temperature (10 K). The sample was then thawed, mixed, and irradiated while freezing to generate oxidative DNA damage via the flash-quench technique. Efforts were made to irradiate all samples under identical conditions for 10 seconds. The EPR spectrum of the irradiated sample was then re-measured under identical instrument settings. All spectra shown in Figure 5 have had an individual DC subtracted; thus, all features are a function of irradiation.

In a sample containing 20 μM Dps loaded with 12 Fe(II)/Dps, poly(dGdC)$_2$ at a concentration of 1 mM base-pairs, 20 μM non-covalent [Ru(phen)(dppz)(bpy′)]$^{2+}$ and 120 μM [Co(NH$_3$)$_5$Cl]$^{2+}$ in a buffer of 50 mM Tris, pH 7.0, 150 mM NaCl, 5% glycerol, a split nearly isotropic signal at g = 4.3 is observed upon irradiation (Figure 5). Comparison with the chemically oxidized sample indicates that this species corresponds to oxidized ferric iron at the mononuclear ferroxidase site in Dps. In contrast, no signal was observed in a sample lacking DNA (Minus DNA) and an attenuated signal was observed in an irradiated sample that contained ferrous iron-loaded Dps, poly(dGdC)$_2$, and [Ru(phen)(dppz)(bpy′)]$^{2+}$ but lacked quencher (Light control). Some signal was observed in the Light control sample, even though steady-state room temperature luminescence experiments with mixed-sequence 70-

mer duplex DNA containing covalently tethered $[Ru(phen)(dppz)(bpy')]^{2+}$ indicated that Dps does not quench the ruthenium(II) excited state (*10*). When Apo-Dps is substituted for Dps loaded with ferrous iron, no signal at $g = 4.3$ is observed, confirming protein-bound iron as the origin of this signal. Importantly, when poly(dAdT)$_2$ is substituted for poly(dGdC)$_2$, the observed signal is significantly attenuated, suggesting that guanine radical plays a role in Dps oxidation. When the dark control subtracted spectra are quantified by double integration over the range of 1400 to 1700 gauss, the signal is attenuated with poly(dAdT)$_2$ by 3-fold. Overall, similar results were obtained in four separate trials.

The wide EPR spectrum of the poly(dGdC)$_2$ with ferrous iron-loaded Dps sample from 500 to 4500 gauss shows that the only features evident upon irradiation are the $g = 4.3$ feature previously discussed and a small signal at $g = 2$ (Figure 6). The $g = 2$ signal is likely an organic radical, either guanine radical or tryptophan radical; however, we were unable to obtain reproducible results at $g = 2$. Despite investigating different temperatures and microwave powers to prevent power saturation, signals at $g = 2$ were too small for conclusions to be drawn. While the tryptophan radical (W52) has been previously observed in *E. coli* Dps with UV-Visible stopped flow experiments (*21*), it is unclear whether we have both the time resolution and sufficient yields to observe this radical with EPR.

In Tris buffer, there is a signal at $g = 4.3$ when a sample of ferrous iron only is mixed with ferricyanide (Figure 7). Therefore, it is important to control for oxidized iron remaining bound to Dps. One approach is to compare samples prepared in a MOPS buffer. In MOPS buffer, no signal is observed when a sample of ferrous iron only is mixed with

ferricyanide (Figure 8). However, a small, un-split signal is apparent at $g = 4.3$ in a sample of ferrous iron-loaded Dps, poly(dGdC)$_2$ DNA, ruthenium complex and diffusing quencher upon irradiation. While the significantly smaller signals in MOPS buffer makes comparisons between samples (i.e., different DNAs) difficult, this MOPS result suggests that at least some of the iron in Tris samples remains bound to the protein after oxidation.

Therefore, in these experiments we have used EPR to spectroscopically confirm the oxidation of WT ferrous iron-loaded *E. coli* Dps following DNA photooxidation with the flash-quench technique. Because Dps is loaded with one ferrous iron per ferroxidase site, this oxidation is evidenced by the appearance of mononuclear ferric iron species of low symmetry at an apparent *g*-value of 4.3. This signal is absent in a Minus DNA control, and attenuated in a Light control which lacks the diffusing quencher necessary for flash-quench. Additionally, guanine radical seems to facilitate Dps oxidation. When poly(dGdC)$_2$ is substituted with poly(dAdT)$_2$ DNA, the yield of Dps oxidation is decreased significantly. Back electron transfer (BET) processes continually decrease the observed yield of oxidized protein in the flash-quench technique. Adenine radicals would be expected to have short lifetimes compared to the neutral guanine radical, which persists for milliseconds (*11*). Thus, similarly to what was postulated with MutY (*12*), it appears likely that guanine radical formation allows more time for the oxidation of Dps by better competing with rapid BET to the intercalated ruthenium(III) photooxidant, resulting in higher yields of Dps oxidation with guanine radical as an intermediate. Additionally, poorly stacked ATAT tracts do not conduct charge efficiently (*32*); this may also be a factor in the lower yield of protein

oxidation with poly(dAdT)$_2$ DNA. Generally, the more favorable oxidation of Dps by guanine radicals also supports the feasibly of a sequential process, according to our hypothesis of DNA-mediated CT, where after guanine radicals are produced, Dps is oxidized to fill guanine radical holes.

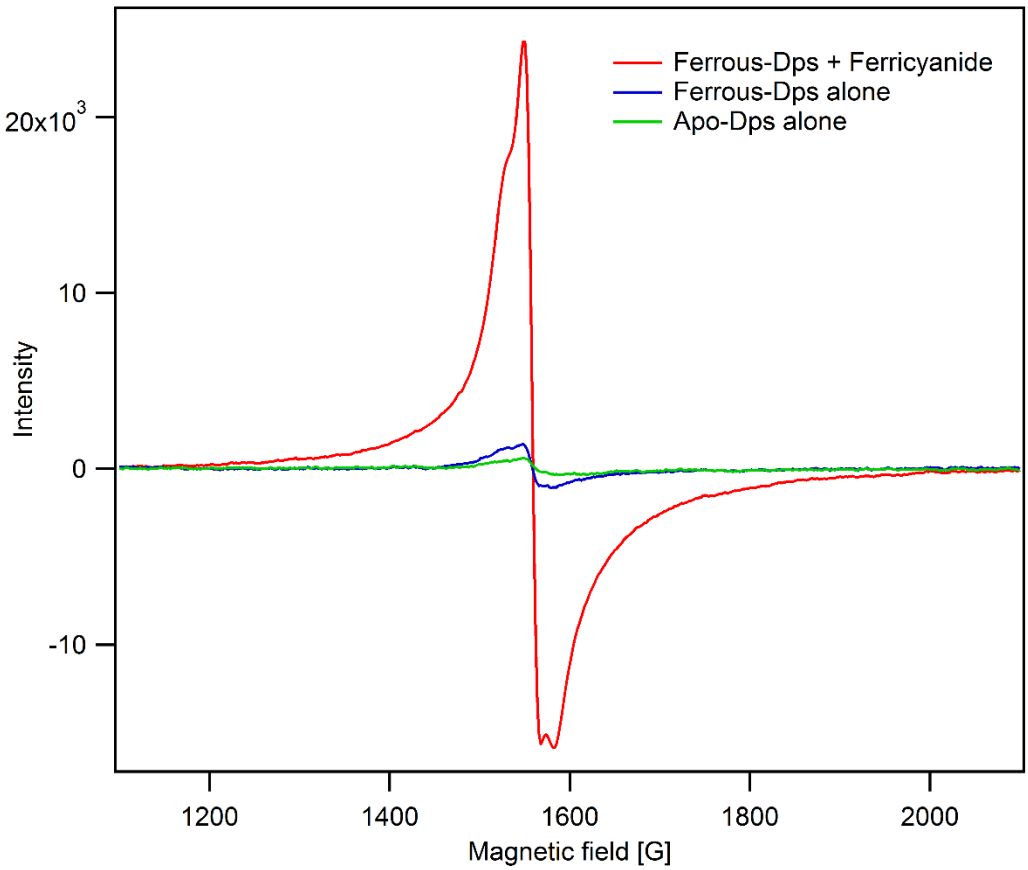

Figure 4. Chemical oxidation of WT *E. coli* Dps containing 12 Fe(II)/Dps with stoichiometric ferricyanide. Conditions: Dps concentration: 20 μM; Actual Fe/Dps: 11.9 ± 0.2; Buffer: 50 mM Tris, pH 7, 150 mM NaCl, 5% glycerol. Instrument settings: modulation amplitude = 10 G at 100 kHz; frequency = 9.373 GHz; microwave power = 6.4 mW; temperature = 10 K. All spectra have had a buffer blank subtracted.

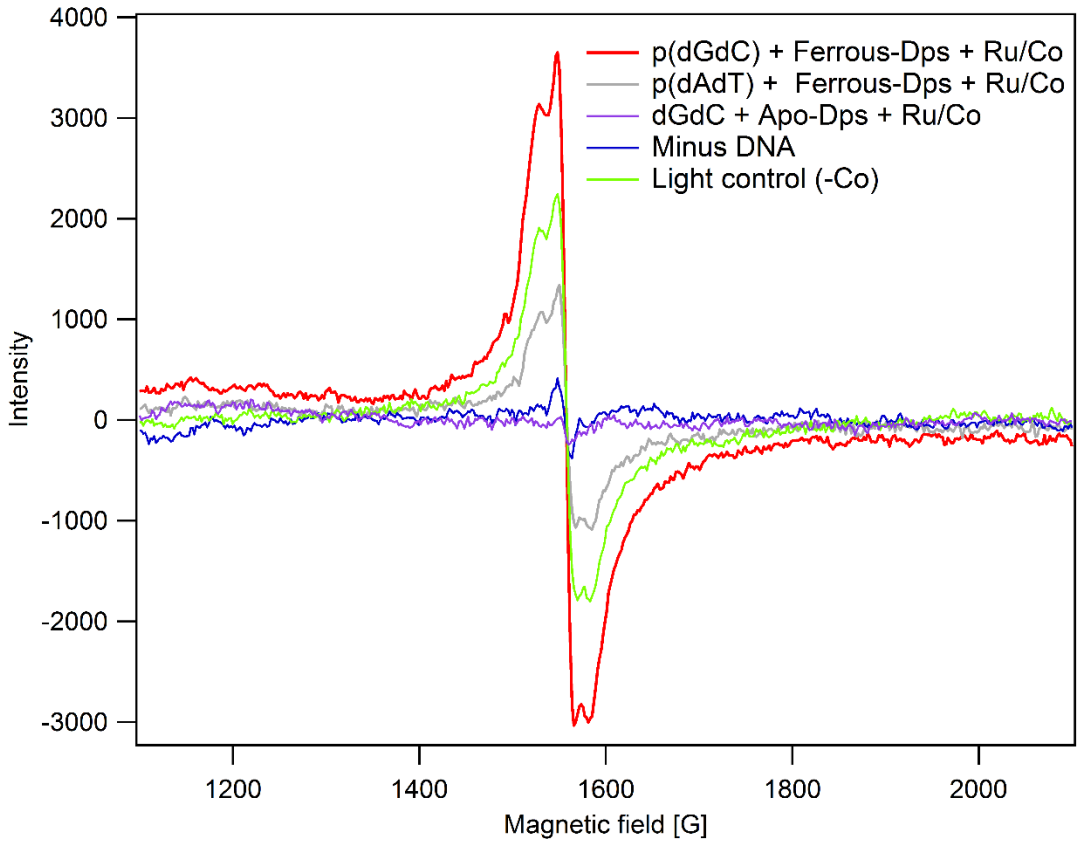

Figure 5. DNA-bound WT *E. coli* Dps oxidation via the flash-quench technique. All spectra have had an individual un-irradiated spectrum subtracted; thus all features are a function of irradiation. Concentrations: 20 μM Dps (Fe^{2+}/Dps: 11.9 ± 0.2), 1 mM base-pairs poly(dGdC)$_2$ or poly(dAdT)$_2$ DNA, 20 μM $[Ru(phen)(dppz)(bpy')]^{2+}$, 120 μM $[Co(NH_3)_5Cl]^{2+}$. Buffer: 50 mM Tris, pH 7.0, 150 mM NaCl, 5% glycerol. Minus DNA sample contains ferrous iron-loaded Dps, Ru, and Co, but lacks DNA; Light control contains ferrous iron-loaded Dps, poly(dGdC)$_2$ DNA, and Ru, but lacks Co quencher. Instrument settings: modulation amplitude = 10 G at 100 kHz; frequency = 9.37 GHz; microwave power = 6.4 mW; temperature = 10 K.

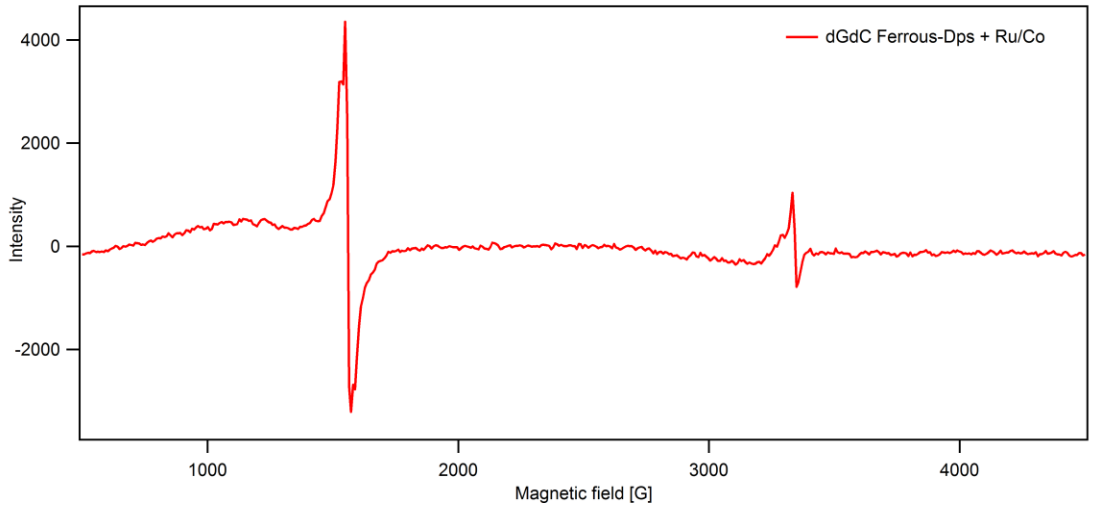

Figure 6. Wide EPR spectra of irradiated sample containing WT ferrous iron-loaded Dps, poly(dGdC)$_2$ DNA, Ru(phen)(dppz)(bpy′)]$^{2+}$, and [Co(NH$_3$)$_5$Cl]$^{2+}$ with dark control subtracted. All conditions and instrument settings identical to Figure 5.

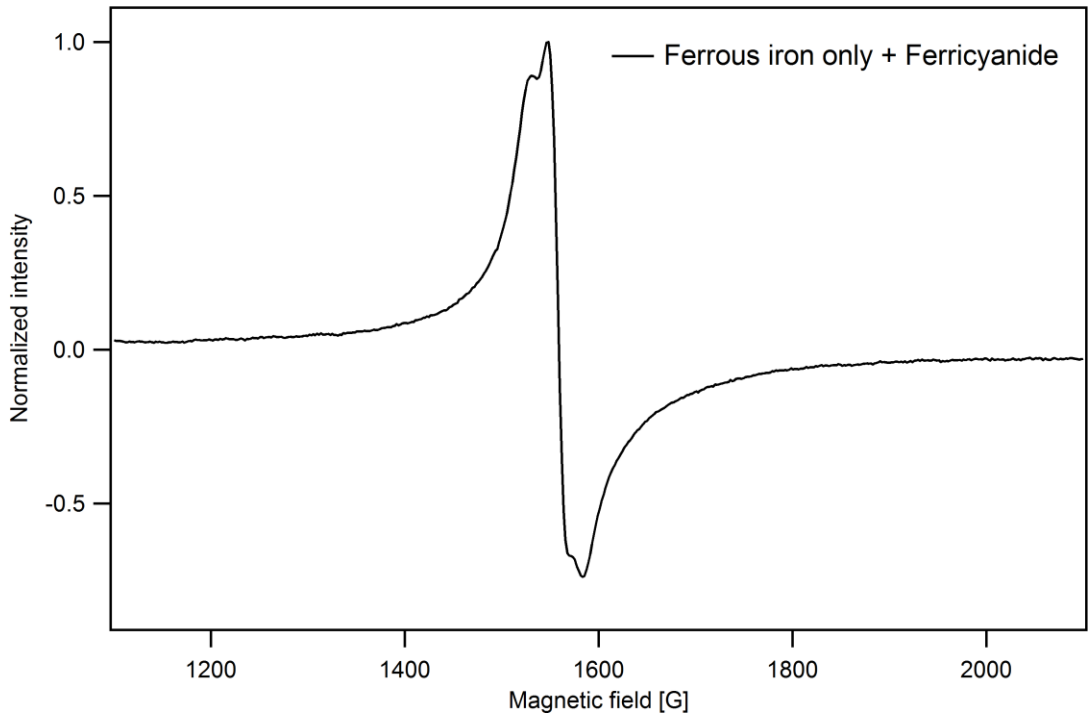

Figure 7. Ferrous iron only (no protein) mixed with stoichiometric ferricyanide in 50 mM Tris, pH 7.0, 150 mM NaCl, 5% glycerol. Concentration of iron was 240 μM, equivalent to that in 20 μM solution of Dps with 12 Fe/Dps. Instrument settings identical to Figure 5.

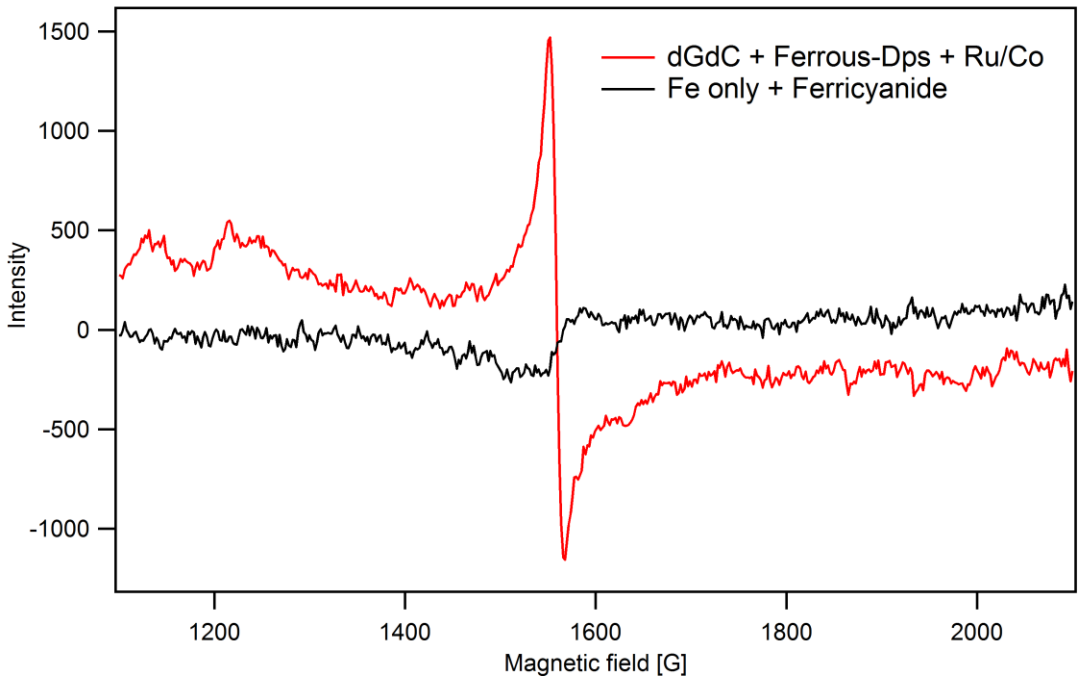

Figure 8. WT Dps EPR spectra compared to Fe only control in MOPS buffer. Concentrations: Fe only: 240 µM ferrous iron with 240 µM ferricyanide (black trace). Irradiated Dps sample: 20 µM Dps (Fe^{2+}/Dps: 11.7 ± 0.1), 1 mM base-pairs poly(dGdC)$_2$ DNA, 20 µM $[Ru(phen)(dppz)(bpy')]^{2+}$, 120 µM $[Co(NH_3)_5Cl]^{2+}$ (red trace). Buffer: 50 mM MOPS, pH 7.0, 150 mM NaCl, 5% glycerol. Dps spectrum has had DC subtracted. Instrument settings: modulation amplitude = 10 G at 100 kHz; frequency = 9.37 GHz; microwave power = 6.4 mW; temperature = 10 K.

3.3.3 EPR results comparing WT Dps with W52 mutants

The ability of ferrous iron-loaded W52A and W52Y Dps to be oxidized by ferricyanide, a diffusing oxidant, was first explored with EPR. Figure 9 shows oxidation of the W52 mutants compared to WT with equivalent moles of ferricyanide, with the EPR intensity adjusted for iron loading (i.e., Intensity / (Fe_{W52A}/Fe_{WT})). When the intensity of the EPR signal resulting from ferricyanide oxidation is adjusted for iron loading in this manner, the W52 mutants show similar yields of iron oxidation to WT Dps, with W52Y showing a slightly increased signal relative to WT. This result indicates that oxidation of the mononuclear iron site by a diffusing oxidant is not affected for W52A and W52Y Dps. Steady-state UV-Visible experiments with the W52 mutants upon oxidation with ferricyanide could be performed to confirm these EPR results.

Next, the X-band EPR spectra of ferrous iron-loaded WT *E. coli* Dps was compared to W52A and W52Y Dps upon DNA photooxidation with the flash-quench technique. Samples containing ferrous iron-loaded Dps, poly(dGdC)$_2$ DNA, non-covalent $[Ru(phen)(dppz)(bpy')]^{2+}$ and $[Co(NH_3)_5Cl]^{2+}$ were irradiated for identical lengths of time. The yield of iron oxidation at $g = 4.3$ was attenuated in the W52 mutants compared to the WT protein, even when adjusted for iron loading (Figure 10). Smaller signals are due to a lower modulation amplitude (5 G) compared to the WT spectra reported above (10 G). When the adjusted spectra are quantified by double integration from 1400 to 1600 gauss, the W52A iron signal is 3.4-fold less than WT, while the W52Y signal is 1.8-fold less than WT. The proficiency in oxidation of the iron sites in these W52 Dps mutants by a chemical

oxidant that directly diffuses to the iron site, combined with the deficiency in the yield of iron oxidation upon DNA photooxidation, suggests that W52 could play a role in mediating ET from the iron site to the DNA.

Because (*i*) the intercalating ruthenium photooxidant is a one-electron oxidant, and (*ii*) the mononuclear iron site has a much lower redox potential (as indicated by its oxidation by ferricyanide, 0.43 V versus NHE, *33*) than tryptophan or tyrosine, making it the thermodynamic sink, the deficiency in iron oxidation for these mutants suggests a role for W52 as an electron transfer hopping intermediate rather than a molecular capacitor. Furthermore, as with WT Dps, we do not have the time resolution and sufficient yields to directly observe the tryptophan or tyrosine radical with EPR.

Another important factor to consider is that the dark control EPR spectra (i.e. before irradiation) of the W52 mutants show evidence of Co^{2+} formation, whereas the WT protein does not (Figure 11). The cobalt quencher, $[Co(NH_3)_5Cl]^{2+}$, is a low-spin Co^{3+} d^6 species with $S = 0$. Upon reduction to Co^{2+}, the complex becomes labile, forming $[Co(H_2O)_6]^{2+}$, a high-spin d^7 species with $S = 3/2$ (EPR-active). Therefore, there may be some direct ET from the ferrous mononuclear iron site to the Co^{3+} quencher to yield EPR-active Co^{2+} in these mutants, perhaps because the ferroxidase site is more solvent-accessible. However, there is very little evidence of ferric iron formation in the DC spectrum of the W52A mutant, and in W52Y, a relatively small percentage of the total amount of iron in the sample is oxidized, allowing ample room for an increase upon irradiation. Thus the lower yield of iron oxidation that we observe upon DNA photooxidation with the W52 mutants is

significant, supporting our EPR results that suggest W52 as an electron transfer intermediate in Dps.

While it is readily rationalized how the W52A mutation would inhibit ET by deleting the aromatic residue, why might substitution of tryptophan for an aromatic tyrosine residue have such an effect? Work by Gray and co-workers has revealed that precise tuning of the reduction potential of hopping intermediates is essential for function (*34*,*35*). With tyrosine, the reduction potential can be modulated by adjacent basic amino acids such as His, Asp, or Glu that can hydrogen bond with the OH group of tyrosine (*35*). In *E. coli* Dps, no basic residues are in the vicinity of Y52 except for the ferroxidase site ligands, which are presumably coordinating iron. Therefore the Dps protein environment may support a tryptophan radical but not be as amenable to a tyrosine radical at the reduction potentials necessary for a hopping intermediate.

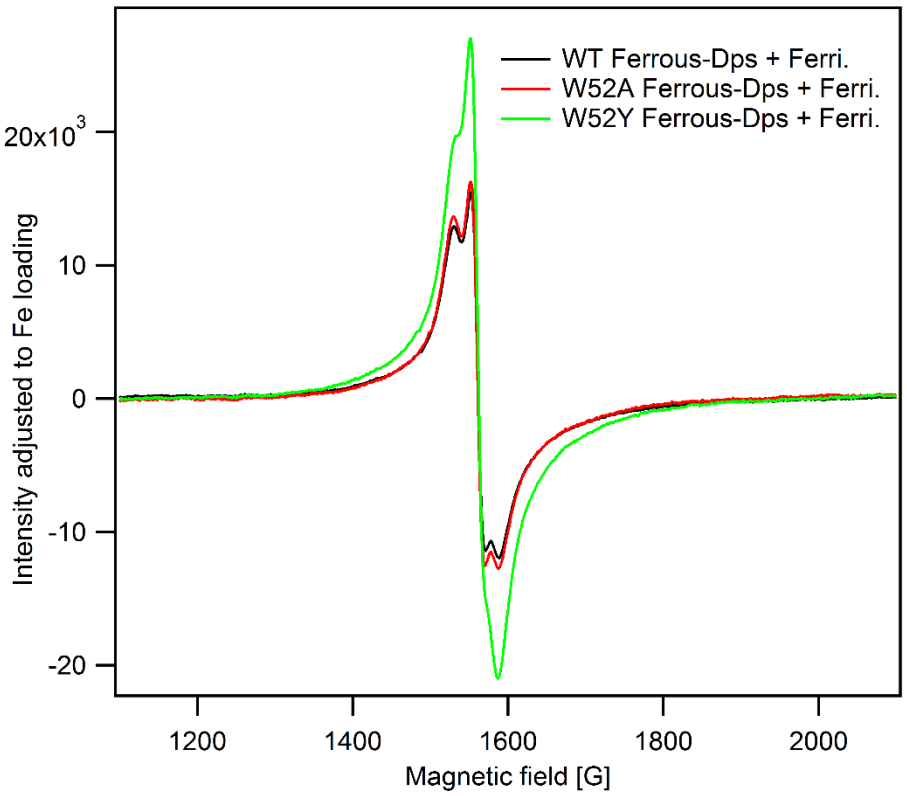

Figure 9. Chemical oxidation of ferrous iron-loaded WT, W52A and W52Y Dps upon mixing with equivalent moles of ferricyanide, with intensity adjusted for iron loading. Intensity was adjusted to that of the WT protein via dividing by the ratio Fe_{W52}/Fe_{WT}. Concentrations: 30 µM Dps (Fe^{2+}/Dps: WT: 13.0 ± 0.4, W52A: 8.9 ± 0.3; W52Y: 10.0 ± 0.1), 60 µM ferricyanide. Buffer: 50 mM Tris, pH 7.0, 150 mM NaCl. Instrument settings: modulation amplitude = 10 G at 100 kHz; frequency = 9.37 GHz; microwave power = 6.4 mW; temperature = 10 K.

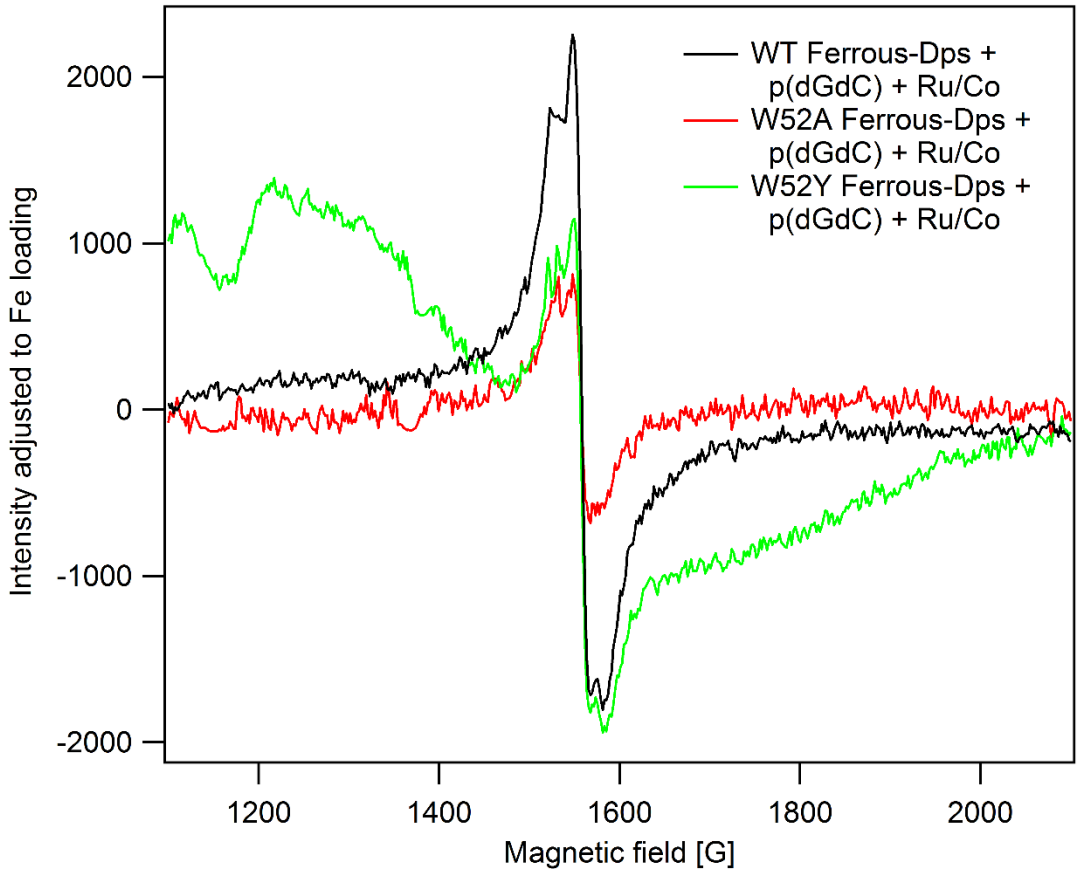

Figure 10. Comparison of ferrous iron-loaded WT Dps and W52A/Y mutant oxidation following DNA photooxidation via the flash-quench technique. All spectra have had an individual un-irradiated spectrum subtracted; thus all features are a function of irradiation. The intensity of the dark-control subtracted W52 spectra was then adjusted to iron loading of the WT protein via dividing by the ratio Fe_{W52}/Fe_{WT}. Concentrations: 20 μM Dps (Fe^{2+}/Dps: WT: 16.0 ± 0.5, W52A: 10.1 ± 0.2; W52Y: 11.5 ± 0.2), 1 mM base-pairs poly(dGdC)$_2$ DNA, 20 μM $[Ru(phen)(dppz)(bpy')]^{2+}$, 120 μM $[Co(NH_3)_5Cl]^{2+}$. Buffer: 50 mM Tris, pH 7.0, 150 mM NaCl, 5% glycerol. Instrument settings: modulation amplitude = 5 G at 100 kHz; frequency = 9.37 GHz; microwave power = 6.4 mW; temperature = 10 K.

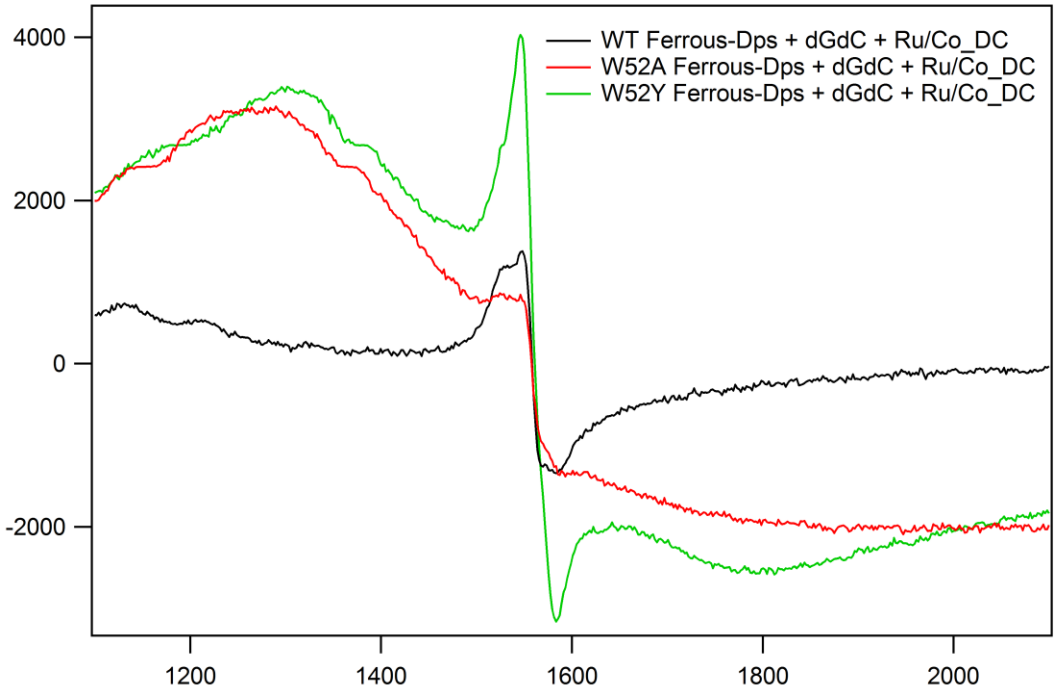

Figure 11. Dark controls (before irradiation) of DNA-bound ferrous iron-loaded WT Dps and W52A/Y mutants. Concentrations: 20 μM Dps (Fe^{2+}/Dps: WT: 16.0 ± 0.5, W52A: 10.1 ± 0.2; W52Y: 11.5 ± 0.2), 1 mM base-pairs poly(dGdC)$_2$ DNA, 20 μM $[Ru(phen)(dppz)(bpy')]^{2+}$, 120 μM $[Co(NH_3)_5Cl]^{2+}$. Buffer: 50 mM Tris, pH 7.0, 150 mM NaCl, 5% glycerol. Instrument settings: modulation amplitude = 5 G at 100 kHz; frequency = 9.37 GHz; microwave power = 6.4 mW; temperature = 10 K.

3.3.4 Hydrogen peroxide survival assay

The survival of *E. coli* upon exposure to hydrogen peroxide was investigated for cells containing WT, W52A, or W52Y Dps. The *dps* knockout *E. coli* strain (*dps*::*kan* Δ*recA* Δ*ara*) (ZK2471) was transformed with a pBAD18 plasmid containing either the *E. coli* WT, W52A, or W52Y *dps* gene under the control of an inducible promoter. Adapted from the method of Martinez and Kolter (*25*), cells were grown overnight and diluted into fresh media with the addition of either the inducer (+), L-arabinose, or sterile water (-). Cells were then grown to exponential phase (OD_{600} = 0.3-0.4) and challenged with varying concentrations of hydrogen peroxide. After stopping the reaction with catalase, cells were diluted and plated in order to quantify colony forming units (CFU). The results from two trials using a 0.2% w/v concentration of L-arabinose inducer are shown in Figure 12. Each data set (i.e., WT Dps induced, 0 – 50 mM hydrogen peroxide) was normalized to the number of colonies on the no hydrogen peroxide plate. The number of normalized colonies under each condition for each trial is shown as an individual point, with the filled markers representing cells with Dps induced and the open markers representing cells with Dps un-induced.

Like was previously observed (*25*), there is a clear difference in bacterial survival upon increasing concentrations of hydrogen peroxide between cells where WT Dps is induced compared to un-induced cells. Overall, cells containing WT Dps survived the hydrogen peroxide challenge best, as can be clearly seen in the inset of Figure 12, with surviving colonies at the highest concentration of hydrogen peroxide. Cells containing

W52Y Dps survive the hydrogen peroxide challenge more effectively than those with W52A Dps, which died off almost as quickly as the un-induced cells. This trend is similar to what was observed in EPR experiments, where the largest attenuation in the yield of iron oxidation following DNA photooxidation was seen with W52A Dps. Thus, W52 is important for cells containing Dps to survive this hydrogen peroxide challenge. In light of our EPR studies on the W52 Dps mutants, where we saw a difference in proficiency between chemical oxidation by a diffusing oxidant and oxidation following DNA photooxidation, some of this *in vivo* effect could be due to inhibition of the DNA-mediated oxidation of Dps upon mutation of W52.

Perhaps the tyrosine residue in W52Y Dps can yet act as a molecular capacitor inside cells, preventing reactive oxygen species (ROS) formation in the hydrogen peroxide oxidation of mononuclear iron sites. Therefore, a one-electron oxidant like $[Rh(phi)_2bpy]^{3+}$ may further elucidate the possible ET role of Dps W52 *in vivo*. The photooxidant $[Rh(phi)_2bpy]^{3+}$ does not require a diffusing quencher and selectively oxidizes DNA rather than producing ROS (*7*). This Rh complex has been previously used successfully to demonstrate SoxR and p53 oxidation within cells as a result of DNA photooxidation (*36*,*37*).

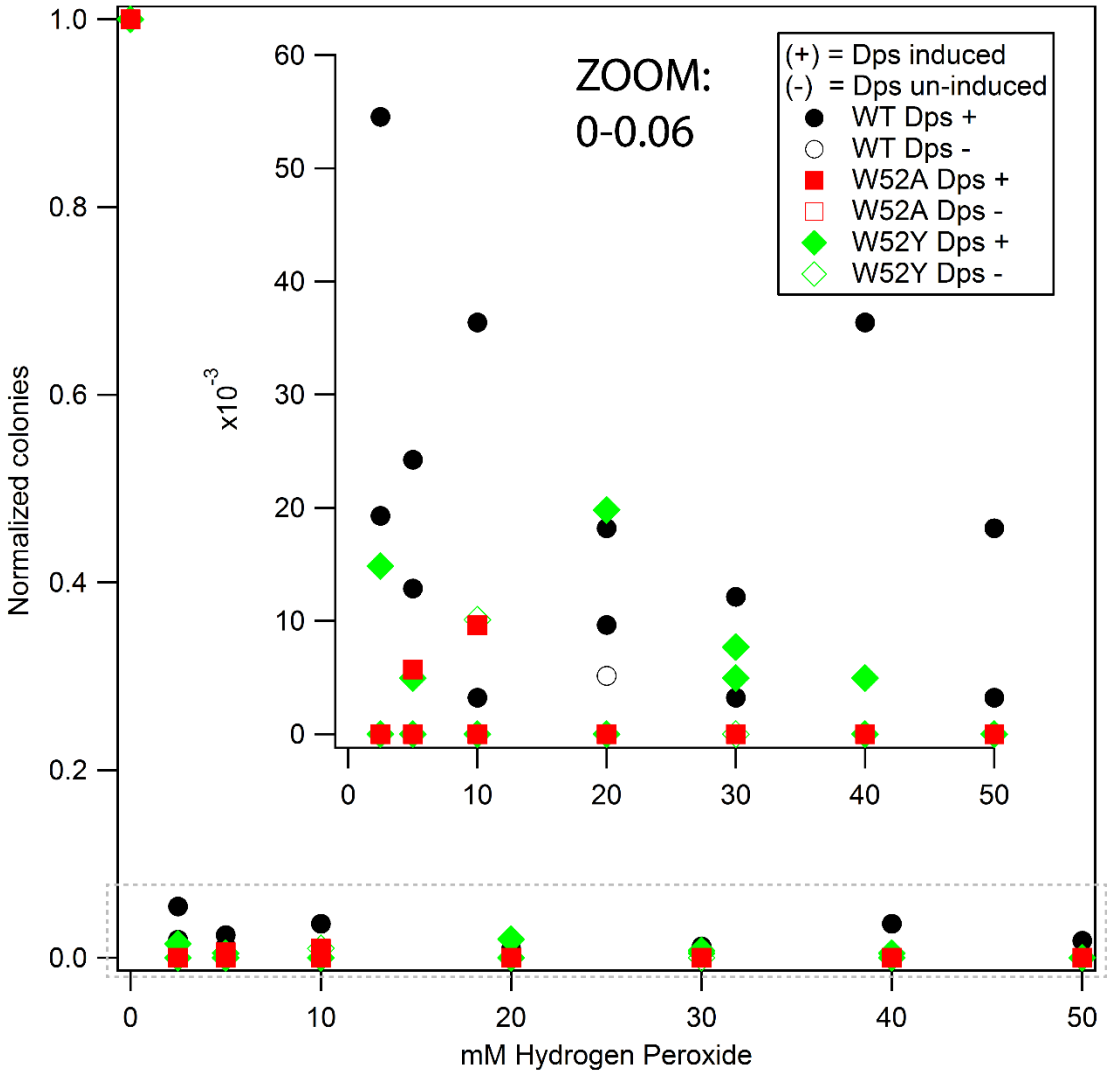

Figure 12. Hydrogen peroxide survival assay comparing *E. coli* with WT (black), W52A (red) or W52Y (green) Dps, where Dps has been either induced with 0.2% w/v L-arabinose (+, filled markers) or not induced (-, open markers). Each data set (i.e., WT Dps induced, 0 – 50 mM hydrogen peroxide) was normalized to the number of colonies on the no hydrogen peroxide plate. Inset is a zoom of the region shown in the gray dashed box (0 – 0.06 normalized colonies).

3.4 Conclusions

We have used EPR to spectroscopically confirm the oxidation of WT ferrous iron-loaded *E. coli* Dps following DNA photooxidation with the flash-quench technique. When poly(dGdC)$_2$ is substituted with poly(dAdT)$_2$ DNA, the yield of Dps oxidation as evidenced by mononuclear ferric iron species at an apparent *g*-value of 4.3, is decreased 3-fold, indicating that guanine radicals facilitate Dps oxidation. Because of the longer lifetime of the guanine radical, its formation likely allows more time for Dps oxidation by better competing with rapid BET to the intercalated ruthenium(III) oxidant produced by flash-quench. The more favorable oxidation of Dps by guanine radicals also supports the feasibility of our hypothesis of a long-distance protection mechanism via DNA CT where Dps is oxidized to fill guanine radical holes in the bacterial genome produced by ROS.

In 12-mer Dps proteins, there is a conserved tryptophan residue in close proximity to the ferroxidase site (W52 in the *E. coli* protein), whereas 24-mer ferritins contain a conserved tyrosine residue. In both cases, this aromatic residue has been proposed to act as a molecular capacitor, providing an extra electron during iron oxidation in order to prevent formation of oxygen radicals (*21*,*23*). The location of the conserved tryptophan residue in Dps proteins between the ferroxidase site and protein surface suggests a possible role as ET hopping intermediate in the DNA-mediated oxidation of the iron site. Here we use site-directed mutagenesis, creating W52A and W52Y *E. coli* Dps, to investigate this possibility. While overall protein folding seems unaffected by these mutations, iron binding is somewhat attenuated. When adjusted for iron loading, the yield of Dps oxidation by a diffusing

oxidant, ferricyanide, was not attenuated by these W52 mutations. However, even adjusted for iron loading, the level of iron oxidation observed in EPR experiments upon DNA photooxidation for both W52A and W52Y Dps is attenuated with respect to the WT protein, suggesting that W52 may play a role in mediating ET from the iron site to DNA. Because the intercalating ruthenium photooxidant used in these experiments is a one-electron oxidant, the deficiency in iron oxidation for these mutants suggests a role for W52 as an electron transfer hopping intermediate rather than a molecular capacitor. The reduction potentials may be precisely tuned to depend on tryptophan as a hopping intermediate, with the result that the tyrosine mutation is disruptive to ET.

We also probe the role of *E. coli* W52 Dps in cells using a hydrogen peroxide survival assay. Cells containing WT Dps survived the hydrogen peroxide challenge best. Whereas there was some attenuation in survival for cells containing W52Y Dps, W52A Dps cells died off almost as quickly as cells that lacked Dps altogether. In view of our EPR studies, some of this *in vivo* effect could be due to inhibition of the DNA-mediated oxidation of Dps upon mutation of W52. Perhaps this tyrosine residue can still act as a molecular capacitor inside cells, preventing ROS formation in the hydrogen peroxide oxidation of mononuclear iron sites. Therefore, a one-electron oxidant like $[Rh(phi)_2bpy]^{3+}$ may further elucidate the possible ET role of Dps W52 *in vivo*.

Interestingly, Dps seems to act as a checkpoint during oxidative stress to delay the initiation of DNA replication in *E. coli* until oxidative DNA damage has been repaired (*38*). Specifically, Chodavarapu *et al.* have shown that Dps interacts with DnaA, inhibiting DnaA-

dependent unwinding of the chromosomal origin (oriC). Thus elevated levels of Dps induced by OxyR under oxidative stress conditions reduce the frequency of replication initiation (*38*). Their data also suggest that DNA binding of Dps is necessary for the inhibition of oriC unwinding. This raises the question if Dps could be signaling with 4Fe4S cluster-containing DNA processing enzymes as part of this checkpoint inhibition.

While the reduction potentials of the ferroxidase site of *E. coli* Dps are unknown, the potential of the mononuclear iron site is less than that of ferricyanide (0.43 V versus NHE). Additionally, the reduction potentials of the ferroxidase site of *P. furiosus* ferritin have been reported as 210 mV for Fe^{3+}-Fe^{3+} to Fe^{3+}-Fe^{2+} and 50 mV for Fe^{3+}-Fe^{2+} to Fe^{2+}-Fe^{2+} (*39*). Therefore the reduction potentials of the ferroxidase site of Dps may perhaps be in an appropriate range to participate in DNA-mediated signaling with 4Fe4S cluster-containing helicases or base excision repair glycosylase enzymes. One could imagine a model where DNA-bound Dps oxidizes these proteins through DNA CT, causing them to remain bound to the DNA and process in towards lesions in the region of the oriC.

In conclusion, we have spectroscopically confirmed the oxidation of *E. coli* Dps following DNA photooxidation with the flash-quench technique, suggested the possibility of an ET hopping intermediate, and moved towards understanding the role of DNA CT with Dps in inside cells. Clearly further work is necessary to elucidate the possible roles of Dps *in vivo*.

References

1. Chiancone, E.; Ceci, P. The multifaceted capacity of Dps proteins to combat bacterial stress conditions: Detoxification of iron and hydrogen peroxide and DNA binding. *Biochim. Biophys. Acta* **2010**, *1800*, 798-805.

2. Zhao, G.; Ceci, P.; Ilari, A.; Giangiacomo, L.; Laue, T. M.; Chiancone, E.; Chasteen, N.D. Iron and hydrogen peroxide detoxification properties of DNA-binding protein from starved cells. *J. Biol. Chem.* **2002**, *277*, 27689-27696.

3. Ceci, P.; Cellai, S.; Falvo, E.; Rivetti, C.; Rossi, G. L.; Chiancone, E. DNA condensation and self-aggregation of *Escherichia coli* Dps are coupled phenomena related to the properties of the N-terminus. *Nucleic Acids Res.* **2004**, *32*, 5935-5944.

4. Wolf, S.G.; Frenkiel, D.; Arad, T.; Finkel, S.E.; Kolter, R.; Minsky, A. DNA protection by stress-induced biocrystallization. *Nature* **1999**, *400*, 83-85.

5. Grodick, M.A.; Muren, N.B.; Barton, J.K. DNA charge transport within the cell. *Biochemistry* **2015**, *54*, 962-973.

6. Saito, I.; Nakamura, T.; Nakatani, K.; Yoshioka, Y.; Yamaguchi, K.; Sugiyama, H. Mapping of the hot spots for DNA damage by one-electron oxidation: Efficacy of GG doublets and GGG triplets as a trap in long-range hole migration. *J. Am. Chem. Soc.* **1998**, *120*, 12686-12687.

7. Hall, D.B.; Holmlin, R.E.; Barton, J.K. Oxidative DNA damage through long-range electron transfer. *Nature* **1996**, *382*, 731-735.

8. Arkin, M.R.; Stemp, E.D.A.; Pulver, S.C.; Barton, J.K. Long-range oxidation of guanine by Ru(III) in duplex DNA. *Chem. Biol.* **1997**, *4*, 389-400.

9. Slinker, J.D.; Muren, N.B.; Renfrew, S.E.; Barton, J.K. DNA charge transport over 34 nm. *Nat. Chem.* **2011**, *3*, 228-233.

10. Arnold, A.R.; Barton, J.K. DNA protection by the bacterial ferritin Dps via DNA charge transport. *J. Am. Chem. Soc.* **2013**, *135*, 15726-15729.

11. Stemp, E.D.A.; Arkin, M.R.; Barton, J.K. Oxidation of guanine in DNA by $Ru(phen)_2(dppz)^{3+}$ using the flash-quench technique. *J. Am. Chem. Soc.* **1997**, *119*, 2921-2925.

12. Yavin, E.; Boal, A.K.; Stemp, E.D.A.; Boon, E.M.; Livingston, A.L.; O'Shea, V.L.; David, S.S.; Barton, J.K. Protein-DNA charge transport: Redox activation of a DNA repair protein by guanine radical. *Proc. Nat. Acad. Sci. USA* **2005**, *102*, 3546-3551.

13. Su, M.; Cavallo, S.; Stefanini, S.; Chiancone, E.; Chasteen, N.D. The so-called *Listeria innocua* ferritin is a Dps protein. Iron incorporation, detoxification, and DNA protection properties. *Biochemistry* **2005**, *44*, 5572-5578.

14. Zhao, G.; Ceci, P.; Ilari, A.; Giangiacomo, L.; Laue, T.M.; Chiancone, E.; Chasteen, N.D. Iron and hydrogen peroxide detoxification properties of DNA-binding protein from starved cells. *J. Biol. Chem*. **2002**, *277*, 27689–27696.

15. Schwartz, J.K.; Liu, X.S.; Tosha, T.; Diebold, A.; Theil, E.C.; Solomon, E.I. CD and MCD spectroscopic studies of the two Dps miniferritin proteins from *Bacillus anthracis*: Role of O_2 and H_2O_2 substrates in reactivity of the diiron catalytic centers. *Biochemistry* **2010**, *49*, 10516-10525.

16. Bou-Abdallah, F.; Chasteen, N.D. Spin concentration measurements of high-spin (g'=4.3) rhombic iron(III) ions in biological samples: theory and application. *J. Biol. Inorg. Chem*. **2008**, *23*, 15-24.

17. Gibson, J.F. EPR of iron in biological systems. In *ESR and NMR of Paramagnetic Species in Biological and Related Systems*. Bertini, I., Drago, R.S., Eds.; Springer: Netherlands, 1979, pp 225-253.

18. Sun, S.; Chasteen, N.D. Rapid kinetics of the EPR-active species formed during initial iron uptake in horse spleen apoferritin. *Biochemistry* **1994**, *33*, 15095-15102.

19. Hayden, J.A.; Hendrich, M.P. EPR spectroscopy and catalase activity of manganese-bound DNA-binding protein from nutrient starved cells. *J. Biol. Inorg. Chem*. **2010**, *15*, 729-736.

20. Nguyen, K.H.; Smith, L.T.; Xiao, L.; Bhattacharyya, G.; Grove, A. On the stoichiometry of *Deinococcus radiodurans* Dps-1 binding to duplex DNA. *Proteins* **2012**, *80*, 713-721.

21. Bellapadrona, G.; Ardini, M.; Ceci, P.; Stefanini, S.; Chiancone, E. Dps proteins prevent Fenton-mediated oxidative damage by trapping hydroxyl radicals within the protein shell. *Free Radical Bio. Med*. **2010**, *48*, 292-297.

22. Chen-Barrett, Y.; Harrison, P. M.; Treffry, A.; Quail, M. A.; Arosio, P.; Santambrogio, P.; and Chasteen, N. D. Tyrosyl radical formation during the oxidative iron deposition in the human apoferritin. *Biochemistry* **1995**, *34*, 7847-7853.

23. Ebrahimi, K.H.; Hagedoorn, P.-L.; Hagen, W.R. A conserved tyrosine in ferritin is a molecular capacitor. *ChemBioChem* **2013**, *14*, 1123-1133.

24. Bou-Abdallah, F.; Yang, H.; Awomolo, A.; Cooper, B.; Woodhall, M.R.; Andrews, S.C.; Chasteen, N.D. Functionality of the three-site ferroxidase center of *Escherichia coli* bacterial ferritin (EcFtnA). *Biochemistry* **2014**, *53*, 483-495.

25. Martinez, A.; Kolter, R. Protection of DNA during oxidative stress by the nonspecific DNA-binding protein Dps. *J. Bacteriol.* **1997**, *179*, 5188-5194.

26. David, S.S.; O'Shea, V.L.; Kundu, S. Base-excision repair of oxidative DNA damage. *Nature*, **2007**, *447*, 941-950.

27. Sovenyhazy, K.M.; Bordelon, J.A.; Petty, J.T. Spectroscopic studies of the multiple binding modes of a trimethine-bridged cyanine dye with DNA. *Nucleic Acids Res.* **2003**, *31*, 2561-2569.

28. Anderson P.A.; Deacon, G.B.; Haarmann, K.H.; Keene, F.R.; Meyer, T.J.; Reitsma, D.A.; Skelton, B.W.; Strouse, G.F.; Thomas, N.C.; Treadway, J.A.; White, A.H. Designed synthesis of mononuclear tris(heteroleptic) ruthenium complexes containing bidentate polypyridyl ligands. *Inorg. Chem.* **1995**, *34*, 6145-6157.

29. Kiassen, N.V.; Marchington, D.; McGowan, H.C.E. H_2O_2 determination by the I_3^- method and by $KMnO_4$ titration. *Anal. Chem.* **1994**, *66*, 2921-2925.

30. Grant, R.A.; Filman, D.J.; Finkel, S.E.; Kolter, R.; Hogle, J.M. The crystal structure of Dps, a ferritin homolog that binds and protects DNA. *Nat. Struct. Biol.* **1998**, *5*, 294-303.

31. Kelly, S.M.; Jess, T.J.; Price, N.C. How to study proteins by circular dichroism. *Biochim. Biophysica. Acta* **2005**, *1751*, 119-139.

32. O'Neill, M.A.; Barton, J.K. DNA charge transport: Conformationally gated hopping through stacked domains. *J. Am. Chem. Soc.* **2004**, *126*, 11471-11483.

33. Dutton, P.L. Redox potentiometry: Determination of midpoint potentials of oxidation-reduction components of biological electron-transfer systems. *Methods Enzymol.* **1978**, *54*, 411-435.

34. Shih, C.; Museth, A.K.; Abrahamsson, M.; Blanco-Rodriguez, A.M.; Di Bilio, A.J.; Sudhamsu, J.; Crane, B.R.; Ronayne, K.L.; Towrie, M.; Vlček, A. Jr.; Richards, J.H.; Winkler, J.R.; Gray, H.B. Tryptophan-accelerated electron flow through proteins. *Science* **2008**, *320*, 1760-1762.

35. Warren, J.J.; Winkler, J.R.; Gray, H.B. Redox properties of tyrosine and related molecules. *FEBS Lett*. **2012**, *586*, 596-602.

36. Lee, P.E.; Demple, B.; Barton, J.K. DNA-mediated redox signaling for transcriptional activation of SoxR. *Proc. Natl. Acad. Sci. USA* **2009**, *106*, 13164-13168.

37. Augustyn, K.E.; Merino, E.J.; Barton, J.K. A role for DNA-mediated charge transport in regulating p53: Oxidation of the DNA-bound protein from a distance. *Proc. Natl. Acad. Sci. USA* **2007**, *104*, 18907-18912.

38. Chodavarapu, S.; Gomez, R.; Vicente, M.; Kaguni, J.M. *Escherichia coli* Dps interacts with DnaA protein to impede initiation: a model of adaptive mutation. *Mol. Microbiol*. **2008**, *67*, 1331-1346.

39. Tatur, J.; Hagen, W.R. The dinuclear iron-oxo ferroxidase center of *Pyrococcus furiosus* ferritin is a stable prosthetic group with unexpectedly high reduction potentials. *FEBS Lett*. **2005**, *579*, 4729-4732.